IET Circuits, Devices & Systems, Volume 13, Issue 3, May 2019, pp. 399-405
DOI:10.1049/iet-cds.2018.5091

Dynamic analysis model of a class E² converter for low power wireless charging links

Akram Bati[1], Patrick C.K. Luk[2], Samer Aldhaher[3], Chan H. See[1,4] ✉, Raed A. Abd-Alhameed[4,5], Peter S. Excell[6]

[1]*School of Engineering, University of Bolton, Deane Road, Bolton, BL3 5AB, UK*
[2]*Centre for Power Engineering, Cranfield University, College Road, Cranfield, MK43 0AL, UK*
[3]*Department of Electrical and Electronic Engineering, Imperial College, Kensington, London, SW7 2AZ, UK*
[4]*School of Electrical Engineering and Computer Science, University of Bradford, Bradford, BD7 1DP, UK*
[5]*Department of Communication and Informatics Engineering, Basra University College of Science and Technology, Basra 61004, Iraq*
[6]*Wrexham Glyndwr University, Wrexham, LL11 2AW, UK*
✉ *E-mail: chs1@bolton.ac.uk*

Abstract: A dynamic response analysis model of a Class E^2 converter for wireless power transfer applications is presented. The converter operates at 200 kHz and consists of an induction link with its primary coil driven by a class E inverter and the secondary coil with a voltage-driven class E synchronous rectifier. A seventh-order linear time invariant state-space model is used to obtain the eigenvalues of the system for the four modes resulting from the operation of the converter switches. A participation factor for the four modes is used to find the actual operating point dominant poles for the system response. A dynamic analysis is carried out to investigate the effect of changing the separation distance between the two coils, based on converter performance and the changes required of some circuit parameters to achieve optimum efficiency and stability. The results show good performance in terms of efficiency (90–98%) and maintenance of constant output voltage with dynamic change of capacitance in the inverter. An experiment with coils of the dimension of 53 × 43 × 6 mm^3 operating at a resonance frequency of 200 kHz, was created to verify the proposed mathematical model and both were found to be in excellent agreement.

1 Introduction

Wireless power transfer (WPT) as a means of conveniently recharging consumer products is a growing trend. This is because the number of cordless devices has been rising rapidly and the changing of batteries or the plugging in of directly connected chargers is a burden which is irksome to busy lives: in addition, there is a significant risk of damage to contacts during plugging and unplugging operations. Wireless charging is inherently less efficient, but this is counterbalanced by its convenience and hence means are being sought to minimise energy losses and any other deleterious effects of energy leakage.

For this work, the primary objective was the charging of batteries in electric drones, although other applications for the developed system can be envisaged. The order of magnitude of the desired transferred power was 20 W and the separation distance between charger and receiver was considered to be in the range from 1 to 15 mm.

The central power transfer component of a wireless charger is fundamentally an air-cored AC transformer. Air cores allow the fields to leak very substantially and hence, in terms of the equivalent circuit of a transformer [1, 2], the mutual inductance is relatively low and the self-inductance of the windings is high. To minimise this effect, it is necessary to operate at a much higher frequency than standard power frequencies and also it is desirable to tune out the effect of the self-inductance of the two windings by resonating them with capacitors.

There is an upper limit on the choice of frequency because power oscillators become inefficient above a few hundred kilohertz and rectifiers suffer similar problems. There is also a problem of leakage fields causing interference to radio communication systems, and this may force the use of unlicensed frequencies in the ISM (Industrial, Scientific and Medical) bands. However, the lowest ISM frequency is now 6.765 MHz [3], which is still a challengingly high frequency for efficient power transfer.

WPT technology requires DC-to-DC converters with resonant inductive links for high efficiency [4–12]. These devices use class E inverters and rectifiers to form efficient high-frequency DC/DC resonant converters. In an application of a 100 W, 200 kHz WPT class E^2 converter, the researchers in [4, 13] used a current-driven class E rectifier. On the other hand, in order to improve the efficiency of WPT, other investigators [8–11, 14] proposed a voltage-driven class E rectifier which used MOSFETs instead of diode rectifiers to achieve high efficiency for 20 W devices. However, some applications need a constant output voltage for stable operation of WPT devices [14]. This has limited the application of the works presented in [4, 8–13]. Since the distance between the transmitting circuit and the receiving circuit is not guaranteed to be fixed at a certain value, the power transferred and the output voltage change accordingly. A regulating circuit is then required to maintain a constant output voltage produced from the WPT devices. To combat this problem, the authors in [15] suggested increasing the input voltage; however, this may lead to device breakdown and lower operating efficiencies due to the excessive heat generated. In [16–21] the authors proposed the use of lossy, complex and bulky additional components and also power-consuming active devices for feedback and communications to achieve constant output voltage. Further, the authors in [22, 23] suggested a non-radiative magnetic coupling approach to deliver power more efficiently; but the effective transfer range was basically restricted to one coil diameter unless relay resonators were adopted [24]. In [25, 26] an optimised circuit structure was adopted which is based on series-shunt mixed resonant circuits but these circuits have poor efficiency, especially for long separation distances, despite the complexity of the circuits.

To clarify the differences between the presented work and other published works, Table 1 compares some technical details, i.e. output power, converter type and efficiency, for inductive power transfer.

Published by IET. This is the Author Accepted Manuscript issued with: Creative Commons Attribution Non-Commercial License (CC:BY:NC 4.0).
The final published version (version of record) is available online at DOI:10.1049/iet-cds.2018.5091. Please refer to any applicable publisher terms of use.

Table 1 Eigenvalues and the dominant poles of the four modes of switching

Mode	Eigenvalues	Dominant pole
I	$[-1.0057 - 2.1058 - 0.0219 - 0.0019 \pm j0.0103 - 0.0000018 - 0.0002] \times 10^8$	$s_{d1} = -180$
II	$[-1.0057 - 0.0005 \pm j\,0.0159 - 0.0124 \pm j0.009 - 0.0000018 - 0.0001] \times 10^8$	$s_{d2} = -180$
III	$[-1.2649 \pm j1.289 - 0.0111 \pm j1.8091 - 0.0015 \pm j0.1 - 0.009974] \times 10^6$	$s_{d3} = -9974$
IV	$[-2.1058 - 0.0195 - 0.0031 \pm j0.0147 - 0.00000077 \pm j0.001 - 0.000164] \times 10^8$	$s_{d4} = -16400$

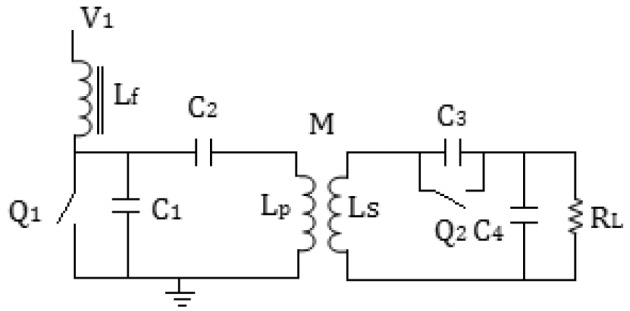

Fig. 1 *Basic circuit of the class E^2 converter*

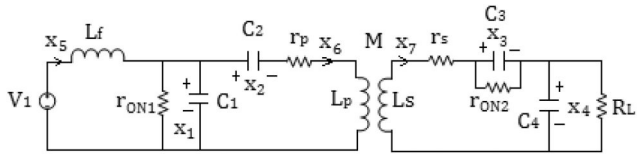

Fig. 2 *Equivalent circuit model of the class E^2 converter*

Examining all the aforementioned methods, it is found that they either have poor efficiency or require high input power and complex structure to maintain a stable output voltage. In order to address these deficiencies, a dynamic analysis model was proposed to explore possibilities to solve this problem, taking into account that a control method is required in the transmitting circuit side that imposes no cost in power consumption and ensures constant output voltage and high efficiency operation. This model was implemented using a MATLAB SIMULINK environment. The aim of this work is to achieve a constant and stable output voltage and the main objectives are

- The examination of the linear time invariant state-space model corresponding to the switching operation of the converter switches.
- Maintaining constant and stable output voltage for variable separation distances.
- Improving the efficiency of the converter by changing the inverter capacitors.

The work included the effect of the variation of circuit parameters on the converter dominant eigenvalues (poles) in the open-loop condition. The complex *s*-plane was adopted in this analysis to identify the effective dominant pole that produces the circuit response under transient changes. For each switching period there is one dominant pole, which can be seen from its position on the complex plane, being the closest one to the imaginary axis. During one complete switching cycle with four transitions of ON-OFFing the MOSFET devices, the circuit will transit through four positions of dominant poles. The effective pole is calculated by using the participation factor and averaging through the four modes of switching positions in each cycle. Handling state-space models of such circuits in this manner makes the design of their controllers and regulators much easier. As a result the circuit will be expected to obtain stable and constant output.

2 Design and methodology

2.1 Mathematical model

The basic circuit is shown in Fig. 1. This can be represented by the following differential equations derived for its equivalent circuit (shown in Fig. 2) based on Kirchhoff's voltage law (KVL) and Kirchhoff's current law (KCL)

$$\dot{v}_1 = \frac{-1}{C_1 r_{Q1}} v_1 + \frac{1}{C_1} i_f + \frac{-1}{C_1} i_p \tag{1}$$

$$\dot{v}_2 = \frac{1}{C_2} i_p \tag{2}$$

$$\dot{v}_3 = \frac{-1}{C_3 r_{Q2}} v_3 + \frac{1}{C_3} i_s \tag{3}$$

$$\dot{v}_4 = \frac{-1}{C_4 R_L} v_4 + \frac{1}{C_4} i_s \tag{4}$$

$$\dot{i}_f = \frac{-r_f}{L_f} i_f + \frac{1}{L_f} V_1 + \frac{v_1}{L_f} \tag{5}$$

$$\begin{aligned} \dot{i}_p = {} & \frac{\alpha L_s}{M^2(1-\alpha)} v_1 + \frac{-\alpha L_p}{M^2(1-\alpha)} v_2 + \frac{-\alpha}{M(1-\alpha)} v_3 \\ & + \frac{-\alpha}{M(1-\alpha)} v_4 + \frac{\alpha r_p L_s}{M^2(1-\alpha)} i_p + \frac{\alpha r_s}{M(1-\alpha)} i_s \end{aligned} \tag{6}$$

$$\begin{aligned} \dot{i}_s = {} & \frac{\alpha}{M(1-\alpha)} v_1 + \frac{-\alpha}{M(1-\alpha)} v_2 + \frac{-\alpha L_p}{M^2(1-\alpha)} v_3 \\ & + \frac{-\alpha L_p}{M^2(1-\alpha)} v_4 + \frac{-\alpha r_p}{M(1-\alpha)} i_p + \frac{\alpha r_s L_p}{M^2(1-\alpha)} i_s \end{aligned} \tag{7}$$

where v_1, v_2, v_3 and v_4 are the voltages across the capacitors C_1, C_2, C_3 and C_4, respectively. It should be noted that v_4 is also the voltage across the load resistor R_L and V_1 is the input voltage. i_f is the inductor current, i_p and i_s are the primary and secondary currents of the transformer, respectively. r_p, L_p, and r_s, L_s are the primary and secondary equivalent series resistances and inductances, respectively, while M is the mutual inductance between them.

A zero equivalent series resistance is assumed for all capacitors. L_f and r_f are the DC-feed inductance and resistance of the inverter, R_L is the load resistor and $\alpha = L_p L_s - M^2$.

In state-space form, (1)–(7) can be transformed into the following matrix form:

Q1

$$\begin{aligned} \dot{x} &= \boldsymbol{A} \cdot \boldsymbol{x} + \boldsymbol{B} \cdot U \\ y &= \boldsymbol{C} \cdot \boldsymbol{x} + \boldsymbol{D} \cdot U \end{aligned} \tag{8}$$

where $\boldsymbol{A}$ is the state matrix, $\boldsymbol{B}$ is the input matrix, $\boldsymbol{C}$ is the output matrix (an identity matrix) and $\boldsymbol{D}$ is the feedforward matrix. $\boldsymbol{x}$ represents the states (variables) vector.

$\boldsymbol{x} = [v_1\ v_2\ v_3\ v_4\ i_f\ i_p\ i_s]^{\mathrm{T}}$, $\boldsymbol{A} = [a_{ij}]$, $\boldsymbol{B} = [b_{ij}], i = 1, \ldots, 7$ and $j = 1, \ldots, 7$

$$\begin{aligned} & U_5 = V_1, \quad \boldsymbol{D} = 0, \quad a_{11} = \frac{-1}{C_1 r_{Q1}}, \quad a_{15} = \frac{1}{C_1}, \quad a_{16} = \frac{-1}{C_1} \\ & a_{26} = \frac{1}{C_2}, \ldots, a_{77} = \frac{\alpha r_s L_p}{M^2(1-\alpha)} \end{aligned} \tag{9}$$

For dynamic analysis, it is assumed that switching ON and OFF of the two MOSFET devices connected across C_1 and C_3 can affect the values of coefficients a_{11} and a_{33} only of the $\boldsymbol{A}$-matrix. When the switch is in ON state, these coefficients have their normal values

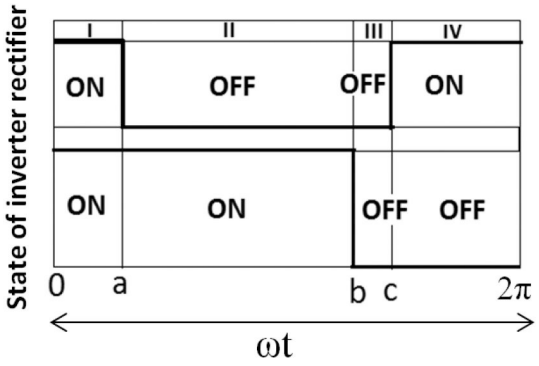

Fig. 3 *Operating modes of the two MOSFETs for one switching cycle*

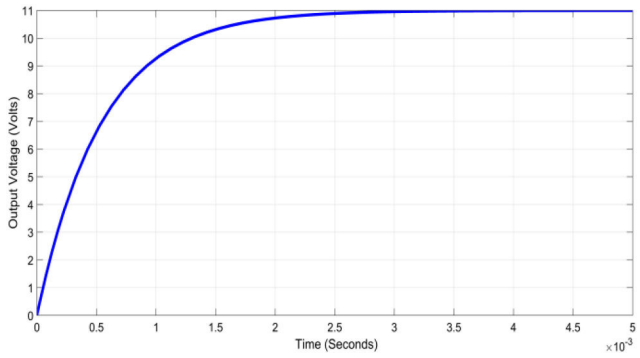

Fig. 4 *Step response of the converter linearised model*

while when they are in their OFF states these two coefficients become zero. In this case, the system transits four states, representing the modes of switching in one cycle, as shown in Fig. 3. The corresponding circuit transfer function (TF) can be described by the following general form:

$$\frac{Y(s)}{U(s)} = \boldsymbol{C}(s\boldsymbol{I} - \boldsymbol{A})^{-1}\boldsymbol{B} \tag{10}$$

where s is the complex operator of the Laplace transform of the system differential equations and $\boldsymbol{I}$ is an identity matrix. $Y(s)$ and $U(s)$ are the Laplace transforms of the output and input, respectively.

The performance of the converter circuit can be determined in terms of the input function U and the initial state of the system $x(0)$ or the initial conditions. The time domain solution can be described by the transition matrix $\boldsymbol{\varphi}(t) = L^{-1}\{[s\boldsymbol{I} - \boldsymbol{A}]^{-1}\}$; the matrices $\boldsymbol{B}$, $\boldsymbol{C}$ are constant matrices and $\boldsymbol{D}$ is a zero matrix. $\boldsymbol{\varphi}(t)$ also involves the inverse Laplace transform of a matrix inversion and the eigenvalues are the solution of the characteristic equation $|sI - A| = 0$.

The four modes of the switching cycle were analysed, based on the position of the dominant poles on the s-plane: these are the nearest poles to the imaginary axis of the s-plane.

A participation factor could be obtained as the ratio of each state time to the cycle period. Then at the end the effective dominant pole was determined by taking the average of the weighted dominant poles of the four states within the switching cycle. For the complex s-plane, the dominant pole can be described by the following complex number:

$$s_{\mathrm{d}} = \sigma \pm \mathrm{j}\omega \tag{11}$$

s_{d} is the dominant pole; σ is the real part of the pole vector and should be negative for a stable system and ω is the imaginary part of the pole vector, also called the damped natural frequency of system response.

$\omega_{\mathrm{n}} = \sqrt{\sigma^2 + \omega^2}$ is the undamped natural frequency and $\zeta = (\sigma/\omega_{\mathrm{n}})$ is the damping ratio of the system.

The system is stable when its dominant pole has a negative real part. The system will have a better transient response if the dominant pole can be shifted to the left and closer to the real axis, i.e. larger σ and smaller ω, meaning higher damping and faster response. This is normally the task of the added controller.

If f_1, f_2, f_3, and f_4 are defined as the participation factors of the dominant poles, where

$$f_1 = \frac{a}{2\pi}, \quad f_2 = \frac{(b-a)}{2\pi}, \quad f_3 = \frac{(c-b)}{2\pi} \text{ and } f_4 = \frac{(2\pi - c)}{2\pi}$$

where a is the time period of the first mode, $(b–a)$ is the time period for the second mode, $(c–b)$ is the time period for the third mode, and the time period for the fourth and last modes is $(2\pi - c)$, as shown in Fig. 3. The effective dominant pole (the average, $s_{d\mathrm{av}}$) can then be found by multiplying each dominant pole of Table 1 by its relevant participating factor and then divided by four which is the number of the operating modes in each switching cycle. The average dominant pole is

$$s_{d\mathrm{av}} = \frac{f_1 s_{d1} + f_2 s_{d2} + f_3 s_{d3} + f_4 s_{d4}}{4} \tag{12}$$

where the calculated participation factors are $f_1 = 0.14951$, $f_2 = 0.350488$, $f_3 = 0.13851$, $f_4 = 0.361489$, and the calculated effective dominant pole, $s_{d\mathrm{av}} = -1850$.

2.2 Eigenvalue analysis and equivalent TF

The eigenvalues of the four switching modes shown in Fig. 3 with their dominant poles are presented in Table 1. These values were obtained from MATLAB based on calculation of the matrix $\boldsymbol{A}$ for each switching period.

The output-to-input voltage ratio of the converter TFs for each mode of switching is given below: (see (13)) . The values in the numerators of (13) are the gains of the TFs. All these TFs do not have zeros but each has seven poles. In Table 1, the second column shows these poles and the dominant poles are shown in column three. The effective eigenvalue or the dominant pole is calculated by using formula (12).

Q2 Now the effective transfer function can be expressed as (see (14)) . This can be reduced to

$$\mathrm{TF}_{\mathrm{av}} = \frac{1850}{(s + 1850)} \tag{15}$$

The dominant pole makes a journey, oscillating between the four modes (positions on the complex s-plane) during each switching

$$\begin{aligned}
\mathrm{TF}_{\mathrm{I}} &= \frac{1.04 \times 10^{19}}{(s+180)(s+2.1\times10^{4})(s+2.2\times10^{6})(s+2\times10^{4})(s+1\times10^{8})(s^2+3.86\times10^{5}\,\mathrm{s}+1.1\times10^{12})} \\
\mathrm{TF}_{\mathrm{II}} &= \frac{1.04 \times 10^{19}}{(s+180)(s+1\times10^{4})(s+1\times10^{6})(s^2+2.5\times10^{6}\,\mathrm{s}+2.3\times10^{12})(s^2+9.7\times10^{4}\,\mathrm{s}+2.5\times10^{12})} \\
\mathrm{TF}_{\mathrm{III}} &= \frac{1.04 \times 10^{19}}{(s+9974)(s^2+3073s+1\times10^{9})(s^2+2.5\times10^{6}\,\mathrm{s}+3.6\times10^{12})(s^2+2.2\times10^{4}\,\mathrm{s}+3.27\times10^{12})} \\
\mathrm{TF}_{\mathrm{IV}} &= \frac{1.04 \times 10^{19}}{(s+2.1\times10^{8})(s+1.9\times10^{6})(s+1.6\times10^{4})(s^2+153.5\,\mathrm{s}+10\times10^{10})(s^2+6.1\times10^{5}\,\mathrm{s}+2.2\times10^{12})}
\end{aligned} \tag{13}$$

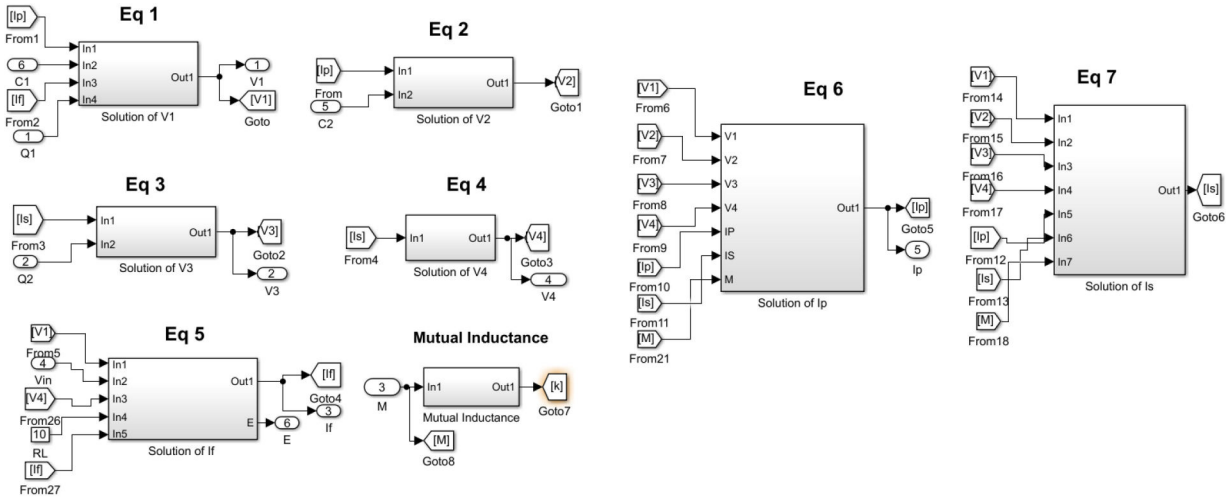

Fig. 5 *Equation models for class E^2 converter*

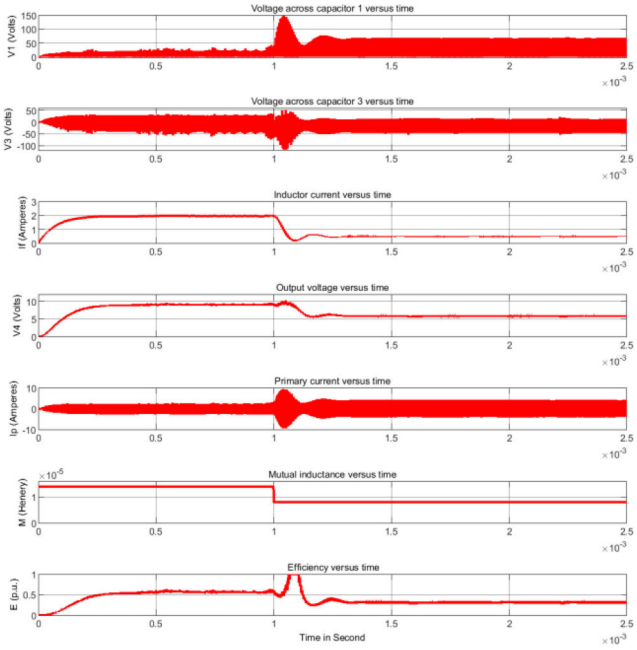

Fig. 6 *Time response of the converter when separation distance changes from 1 to 8 mm at T = 1 ms*

cycle. This method of averaging the position of the dominant pole gives an accurate location for it, depending on the time period for each mode of operation.

The resultant position of the dominant pole $s = -1850$ is obtained from this averaging method. The other poles given in (15) are very far from the imaginary axis of the s-plane and have no effect on the converter response. The corresponding time response of this transfer function is plotted in Fig. 4.

2.3 Linearised SIMULINK model

In order to capture converter dynamics, a linearised mathematical model is necessary to identify system response. It also helps in designing a controller that achieves a constant output. Linearisation of this model was carried out using built-in functions available from MATLAB SIMULINK software which are based on the output and input nodes that need to be identified. To effectively study this, an open-loop class E^2 converter model was established, for which the corresponding equation models can be found in Fig. 5.

3 Simulated results and discussion

3.1 Effect of parameter variation on system dynamic response

Looking at the effective dominant poles given in (13), the circuit remains always stable with some amount of oscillations and this can be seen very clearly when separation distance between the primary and the secondary varies suddenly as this represents the most severe disturbance to the circuit. To better understand this, Fig. 6 depicts the time response variation of V_1 (voltage across capacitor 1), V_3 (voltage across capacitor 3), I_f (inductor current), V_4 (output voltage) and I_p (transformer primary current) when the separation distance is changed from 1 to 8 mm, which is equivalent to changing M (mutual inductance) from 14 to 8 µH at time = 1 ms. As can be clearly seen, when the separation changes, the converter circuit goes through three stages of change, i.e. it builds up its magnetic flux, its transient response and then reaches a new steady-state condition. At the start, the separation distance is kept to its minimum, 1 mm, to see how the converter circuit builds its magnetic field for optimum mutual coupling between the two coils. It is clear from the responses that all variables ($x_1, \ldots, x_7$) reach their steady-state values in 0.54 ms. Then the transformer is disturbed suddenly by changing the separation distance to 8 mm. This represents the most severe potential disturbance to the converter.

Fig. 7 describes the time response of V_1, V_3, V_4, I_f, I_p, M and efficiency when the separation distance is changing repeatedly to different values. These responses show that the converter is sufficiently stable to cope with this type of cyclic disturbance. If the system is not sufficiently stable it will lose its stability with such types of cyclic disturbance. As can be observed, the converter cannot achieve both high output voltage and high efficiency: it needs adaptive parameters to be tuned to maintain its optimal working condition.

3.2 Improving converter efficiency

3.2.1 Changing capacitors C_1 and C_2: Keeping the converter efficiency relatively high is a major challenge for such a circuit with a pre-determined resonance frequency. One of the suggested methods to improve its efficiency is by changing the frequency and/or the duty ratio of the two switching devices. However, this entails the change of capacitor C_3 to meet the desired operating resonant frequency as well as changing the values of capacitors C_1 and C_2 to maximise the efficiency.

Assuming that there is no control access to the receiver side (RS) of the converter, the only way to optimise the efficiency of the

$$\mathrm{TF}_{\mathrm{av}} = \frac{1.04 \times 10^{19}}{(s + 1850)(s + 2.1 \times 10^{8})(s + 2.2 \times 10^{6})(s + 1.64 \times 10^{4})(s^2 + 3.86 \times 10^{5}\,s + 1.1 \times 10^{12})} \tag{14}$$

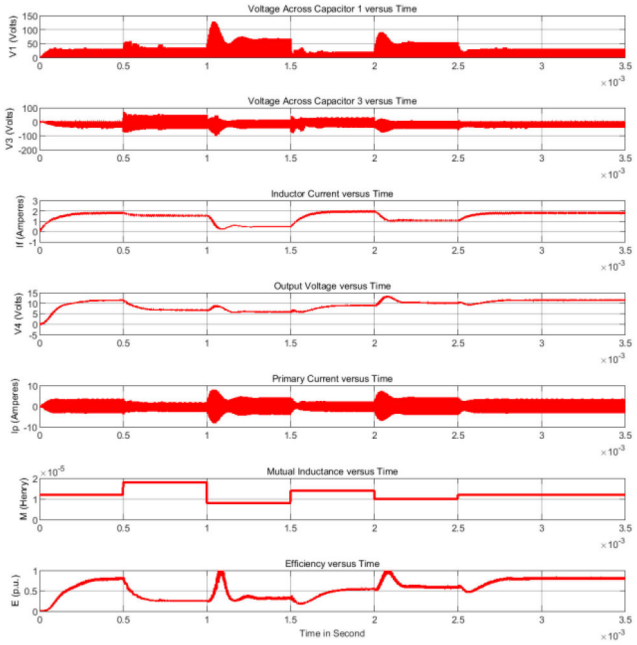

Fig. 7 *Time response of the converter when separation distance changes to different values*

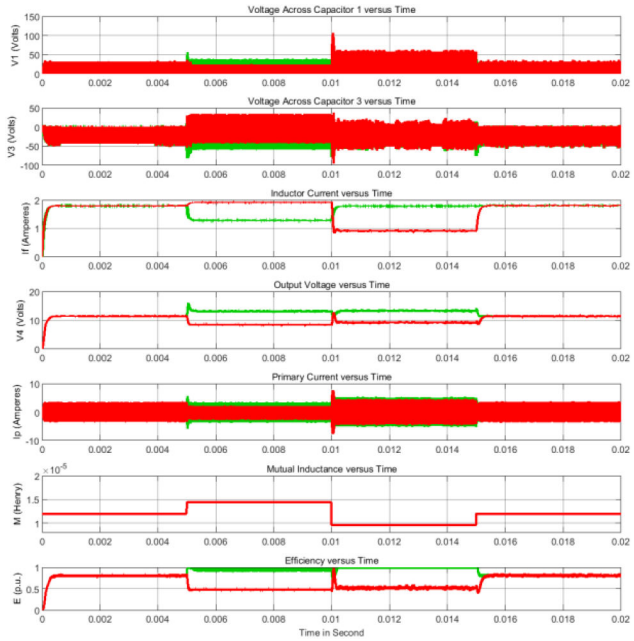

Fig. 8 *Effect of changing C_1 and C_2 on efficiency, red curve indicates the fixed capacitors C_1 and C_2, green curve indicates the tuned capacitors C_1 and C_2*

converter is at the transmitter side (TS). In this study, the values of capacitors C_1 and C_2 were changed simultaneously with the change in separation between the TS and the RS. Interestingly, it was found that, when C_1 and C_2 were increased to 70 and 64 nF, respectively, higher efficiencies ranging from 90 to 98% were achieved with the change in the separation from 1 to 8 mm. This means that resonance is occurring and this leaves the circuit with its inductor and winding resistances, which cause some power loss. This finding is in good agreement with [9]. To further comprehend this, Fig. 8 depicts the efficiency achievement of the converter when C_1 and C_2 were allowed to change simultaneously with changes of separation.

3.2.2 Changing frequency and duty ratio: In contrast to the achievement of good efficiency in the previous section, a change of frequency alone has a deleterious impact on circuit efficiency even

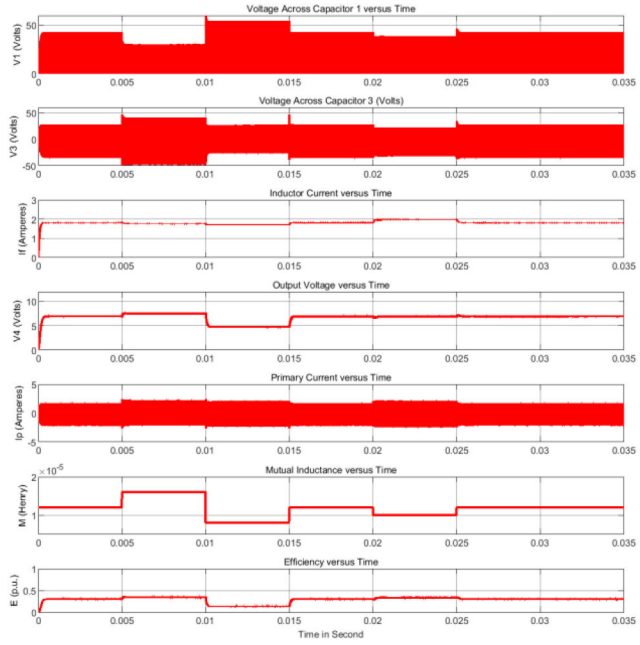

Fig. 9 *Effect of frequency change on circuit efficiency*

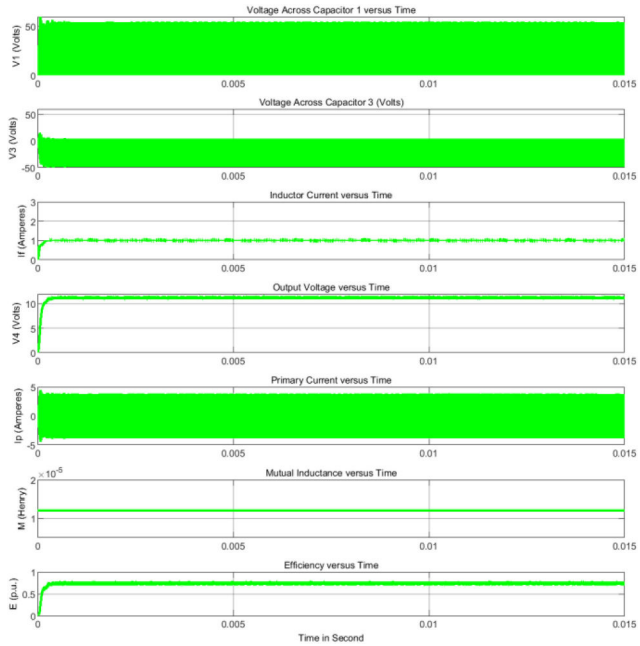

Fig. 10 *Results for the converter when f = 217.243 kHz, R_L = 10 Ω, D1 = 0.444, D_2 = 0.501, delay angle of switch two = 230.1°, k = 0.55, separation = 3 mm*

if the capacitors' values are changed accordingly. To verify this, the operating frequency of the proposed model was changed from 200 to 160 kHz and the capacitors' values were again optimised. As can be seen in Fig. 9, poor efficiency is obtained, only generally around 24% on average. However, if the duty ratios of the two switches are changed simultaneously with the change of frequency, as well as altering the delay angle of switch 2 without changing the values of capacitors 1 and 2, the efficiency starts to improve, as shown in Fig. 10, assuming a fixed separation distance of 3 mm. This leads to a conclusion that changing frequency and duty ratios is another alternative to optimise the efficiency of the converter.

4 Experimental setup and verification

To verify the simulated results, an experiment was set up as shown in Fig. 11 and the corresponding test bed parameters are tabulated in Table 2. The actual voltage across MOSFETs Q_1 and Q_2 as well as the primary and secondary current responses obtained from the

same converter used by Luk *et al.* [9] are verified by the simulation responses obtained from this work, as shown in Fig. 12. These responses also show that the optimum switching frequency is 200 kHz. The class E^2 converter implemented in this work consisted of a class E zero-voltage switching (ZVS) and zero-derivative voltage switching (ZDS) inverter with an infinite DC-feed inductance, an inductive link consisting of primary and secondary coils separated by a certain air gap and a voltage driven class E ZVS rectifier.

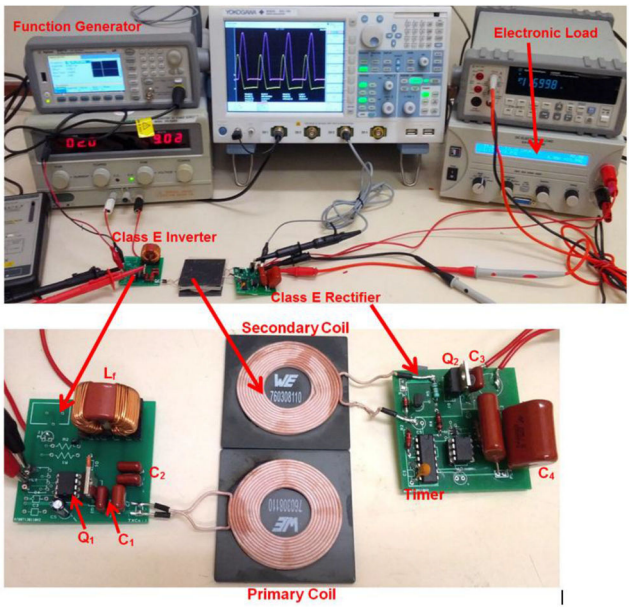

Fig. 11 *Photograph of the experimental setup. Where the dimensions of the Tx and Rx coils are 53 × 43 × 6 mm³, and the dimensions of their associated circuits are similar: 53 × 43 × 20 mm³ (approx.)*

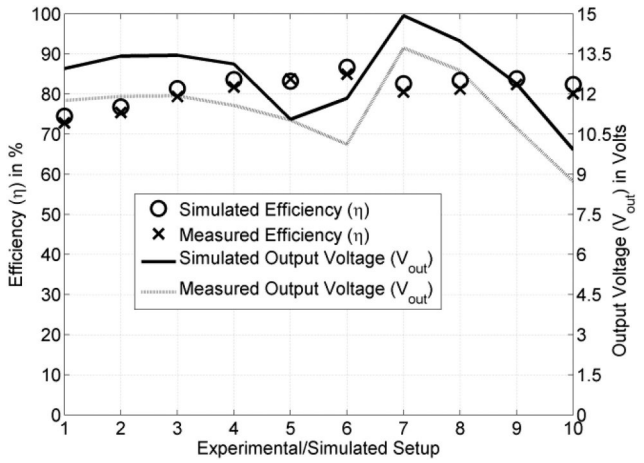

Fig. 12 *Simulated and measured efficiencies and output voltage (V_{out}) of the experiment setups, with parameters as listed in Table 2*

It is mentioned in [27] that efficient class E converter is attributed to its soft-switching capability.

The switch can undergo ZVS and ZDS only at optimum operating conditions. In this work, the ZVS and ZDS conditions are satisfied because the chosen load resistance is changing between 5 and 10 Ω: this is considered to be optimum for this type of converter. Thus the conditions stated in [27] are not violated.

The design procedure begins with coils of the inductive link: these coils should have a large quality (Q) factor at the switching frequency of the converter for maximum power transfer efficiency. Developing coils for inductive links is outside the scope of this paper as there is extensive research that has been devoted to this topic in the literature. For this reason, the popular 'Qi' Wireless Power Consortium standard [28] is adopted to determine the primary and secondary coils. Both coils have a maximum dc resistance of 0.1 Ω, an inductance of 24 µH, and a maximum Q factor of 230 at 200 kHz [29]. The coils' equivalent series resistance can be calculated and is equal to 0.137 Ω. With the addition of the connectors' resistance and the dc resistance of the printed circuit board tracks, the total resistance of the coils is ~0.18 Ω at 200 kHz.

The mutual inductance between the primary and secondary coils can be measured at different separation distances. For a separation distance of 3 mm, the measured mutual inductance is ~12 µH, which corresponds to a coupling coefficient (k) value of 0.50.

The secondary coil of the inductive link and capacitor C_3 form the resonant part of the class E rectifier. The value of C_3 that will cause the rectifier to resonate at 200 kHz is equal to $C_3 = (1/\omega^2 L_p) = 26.38$ nF. The output capacitor C_4 should be large enough to maintain a constant dc voltage. A value of 6.6 µF was found to be suitable. The capacitors used are polypropylene capacitors from EPCOS [30]: according to their datasheet they have a dissipation factor of 0.002. Their ESR's are assumed to be zero. The dimensions of the boards are equal to the coils, which are 53 mm × 43 mm, this is so that the inverter and rectifier boards could be placed behind the coils.

The inverter and rectifier switches are named Q_1 and Q_2, respectively. To drive MOSFET Q_2 of the rectifier additional circuitry is needed to ensure that the switching signal is applied at the correct instants. Referring to the time instant c in Fig. 3, MOSFET Q_2 switches ON once the voltage across it crosses zero volts. Therefore, a comparator is used to trigger the switching signal using the voltage across this MOSFET. On the other hand, the voltage across MOSFET Q_2 cannot be relied on as a trigger to turn it OFF. This is because the voltage has a near-zero time derivative. Therefore, a one-shot timer is used to drive MOSFET Q_2 with a time duration equal to or less than duty cycle D_2. The timer is triggered once the comparator detects a zero crossing in the voltage across MOSFET Q_2.

The ZDS of the class E inverter means that the first derivative of the voltage across switch Q_1 is zero at the moment it is switched ON, which in turn results in zero-current switching. The switches are driven at the same switching frequency, but with different duty cycles.

Table 2 Measurement setup parameters for a variable load and variable coupling coefficient

Setup	R, Ω	k	f, kHz	D_1	D_2	∅	V_{Q1max}, V	V_{Q2max}, V	I_{Q1max}, A	I_{Q2max}, A	I_f, A	I_p, A	V_4, V
1	5	0.5	187.8	0.59	0.582	221.4	38.16	53.46	10.54	5.85	4.22	12.84	11.76
2	6	0.5	190.0	0.571	0.565	223.4	36.59	51.67	8.95	5.06	3.48	11.08	11.91
3	8	0.5	194.7	0.535	0.535	226.9	33.91	47.75	6.72	3.95	2.49	8.6	11.93
4	10	0.5	200.0	0.5	0.511	229.8	31.68	43.73	5.22	3.2	1.82	6.9	11.57
5	12	0.5	205.8	0.465	0.49	232.0	29.75	39.69	4.12	2.64	1.34	5.64	11.02
6	14	0.5	212.6	0.426	0.471	233.4	27.89	35.27	3.24	2.17	0.95	4.61	10.12
7	10	0.45	187.7	0.543	0.519	228.8	34.49	52.79	6.9	3.7	2.6	8.77	13.72
8	10	0.47	192.1	0.526	0.516	229.2	33.37	49.11	6.18	3.5	2.27	7.98	12.87
9	10	0.52	206.1	0.48	0.507	230.1	30.53	40.17	4.63	2.99	1.55	6.24	10.72
10	10	0.55	217.2	0.444	0.501	229.8	28.68	34.59	3.77	2.63	1.16	2.48	8.72

Table 3 Characteristics of published class E rectifiers

Ref.	Output power, W	Converter type	η, %
this work	20	class E^2 converter, 200 kHz	90–98
[9]	20	class E^2 converter, 200 kHz	92.32
[11]	10	class E rectifier, Si Schottky	94
[12]	50	class E power amplifier, 3.45 MHz	80
[13]	100	class E power amplifier, 6 MHz	77
[14]	3	mixed-resonant coupling, 4 MHz	85
[15]	0.02	non-radiative power transfer, 5.256 MHz	36.5–41.8
[16]	50–200	half-wave class E rectifier, 4 MHz	90
[17]	100	class E^2 converter, 200 kHz	85.5

The converter used was connected to a nominal load of 10 Ω with a coupling coefficient of 0.50 and a 200 kHz switching frequency. The duty cycle D_1 was set to 0.50 and the one-shot timer was set to produce a 2.56 µs pulse, corresponding to a duty cycle D_2 of 0.51. The practical and simulation results which show lower efficiencies occur when separation distance between the two coils, selected capacitor values or switching frequencies are not the optimal values.

In Fig. 12, a comparison between the converter efficiency and output voltage for simulated results and those obtained from the experiment is shown, based on the configurations listed in Table 2. Fig. 12 confirms that the simulated and measured results are in good agreement, particularly for the efficiency. There are small percentage errors that are attributable to the tolerance of the capacitors and other components used. It can be concluded that the circuit can achieve high levels of efficiency if the frequency, duty ratios and delay angles of the two switching devices can be altered dynamically.

Table 3 shows the comparisons of the results of this work with other published work in terms of efficiency, taking into account the converter type used. This clearly shows the substantial advance that has been achieved in obtaining efficiencies that are close to the maximum possible for class E^2 converters.

5 Conclusion

A dynamic analysis model of the E^2 WPT converter has been presented. The results suggest the switching process of the MOSFET devices does not have a deleterious effect on the stability of the circuit but changing frequency or duty ratio causes the converter to operate at low efficiencies and this can cause instability. Remarkably, it is found that at a resonance frequency of 200 kHz, the dynamic change of transmitter side capacitors has achieved near-maximal efficiencies (90–98%) and maintained high output voltage. The high efficiency obtained is due to the resonance occurring in the converter by the action of the capacitors that compensate for some power loss in the inductor and windings resistances. The proposed work also suggests further development of optimally self-tuned regulators of such types for use in WPT devices. This can be done by changing the capacitors in the transmitter dynamically with the change in separation distances using a closed-loop control system. The results confirmed that capacitor tuning produces almost stable output voltage and high efficiency. Experimental results verified the mathematical model, suggesting it is a reliable model for optimising the performance of existing open-loop WPT systems.

6 References

[1] Ayachit, A., Kazimierczuk, M.: 'Transfer functions of a transformer at different values of coupling coefficient', *IET Circuits Devices Syst.*, 2016, **10**, (4), pp. 337–348

[2] Kazimierczuk, M., Jozwik, J.: 'Class E^2 narrow-band resonate dc/dc converter', *IEEE Trans. Instrum. Meas.*, 1989, **38**, (6), pp. 1064–1068

[3] OFCOM: '*Frequency bands designated for industrial, scientific and medical use (ISM)*' (UK Office of Communications, 2017)

Q5 [4] Wireless Power Consortium. Available at http://www.wirelesspowerconsortium.com

[5] Kazimierczuk, M.M.K., Bui, X.: 'Class E DC/DC converters with a capacitive impedance inverter', *IEEE Trans. Ind. Electron.*, 1989, **36**, (3), pp. 425–433

[6] Schuylenbergh, K.V., Puers, R.: '*Inductive powering: basic theory and application to biomedical systems*' (Springer-Verlag, New York, 2009)

[7] Qualcomm Halo. Available at http://www.qualcommhalo.com/

[8] Wu, H., Covic, G., Boys, J., *et al.*: 'A series-tuned inductive power-transfer pickup with a controllable AC-voltage output', *IEEE Trans. Power Electron.*, 2011, **26**, (1), pp. 98–109

[9] Luk, P.C.K., Aldhaher, S., Fei, W., *et al.*: 'State-space modelling of class E^2 converter for inductive links', *IEEE Trans. Power Electron.*, 2015, **30**, (6), pp. 3242–3251

[10] Aldhaher, S., Luk, P.C.K., Whidborne, J.: 'Tuning class E inverters applied in inductive links using saturable reactors', *IEEE Trans. Power Electron.*, 2014, **29**, (6), pp. 2969–2978

[11] Aldhaher, S., Luk, P.C.K., Drissi, K., *et al.*: 'High-input-voltage high-frequency class E rectifiers for resonant inductive links', *IEEE Trans. Power Electron.*, 2015, **30**, (3), pp. 1328–1335

[12] Calder, R.J., Lee, S.H., Lorenz, R.D.: 'Efficient, MHz frequency resonant converter for sub-meter (30 cm) distance wireless power transfer'. Proc. IEEE Energy Conversion Congress Exposition, 2013, pp. 1917–1924

[13] Pinucla, M., Yates, D.C., Lucyszyn, S., *et al.*: 'Maximizing DC-to-load efficiency for inductive power transfer', *IEEE Trans. Power Electron.*, 2013, **28**, (5), pp. 2437–2447

[14] Chen, L., Liu, S., Zhou, Y.C., *et al.*: 'An optimizable circuit structure for high efficiency wireless power transfer', *IEEE Trans. Power Electron.*, 2013, **60**, (1), pp. 339–349

[15] Thomas, E.M., Heebl, J.D., Pfeiffer, C., *et al.*: 'A power link study wireless non-radiative power transfer system using resonant shielded loops', *IEEE Trans. Circuits Syst. I*, 2012, **59**, (9), pp. 2125–2136

[16] Birca-Galateanu, S., Cocequerelle, J.L.: 'Class E half-wave low d*v*/d*t* rectifier operating in a range of frequencies around resonance', *IEEE Trans. Circuits Syst. I*, 1995, **42**, (2), pp. 83–94

[17] Nagashima, T., Inoue, K., Wei, X., *et al.*: 'Inductively coupled wireless power transfer with class E^2 DC-DC converter'. 2013 European Conf. on Circuit Theory and Design (ECCTD), September 2013, pp. 1–4

[18] Wang, G., Liu, W., Sivaprakasam, M., *et al.*: 'Design and analysis of an adaptive transcutaneous power telemetry for biomedical implants', *IEEE Trans. Circuits Syst. I*, 2005, **52**, (10), pp. 2109–2117

[19] Chen, Q., Wong, S.C., Tse, C.K., *et al.*: 'Analysis, design, and control of a transcutaneous power regulator for artificial hearts', *IEEE Trans. Biomed. Circuits Syst.*, 2009, **3**, (1), pp. 23–31

[20] Si, P., Hu, A.P., Malpas, S., *et al.*: 'A frequency control method for regulating wireless power to implantable devices', *IEEE Trans. Biomed. Circuits Syst.*, 2008, **2**, (1), pp. 22–29

[21] Moradewicz, A., Kazmierkowski, M.: 'Contactless energy transfer system with FPGA-controlled resonant converter', *IEEE Trans. Ind. Electron.*, 2010, **57**, (9), pp. 3181–3190

[22] Low, Z.N., Chinga, R.A., Tseng, R., *et al.*: 'Design and test of a high-power high-efficiency loosely coupled planar wireless power transfer system', *IEEE Trans. Ind. Electron.*, 2009, **56**, (5), pp. 1801–1812

[23] Casanova, J.J., Low, Z.N., Lin, J.: 'A loosely coupled planar wireless power system for multiple receivers', *IEEE Trans. Ind. Electron.*, 2009, **56**, (8), pp. 3060–3068

[24] Kim, Y.-H., Kang, S.-Y., Lee, M.-L., *et al.*: 'Optimization of wireless power transmission through resonant coupling'. Proc. Compatibility and Power Electronics (CPE), 2009, pp. 426–431

[25] Severns, R.P.: 'Topologies for three- element resonant converters', *IEEE Trans. Power Electron.*, 1992, **7**, (1), pp. 89–98

[26] Chen, L., Liu, S., Zhou, Y.C., *et al.*: 'An optimizable circuit structure for high-efficiency wireless power transfer', *IEEE Trans. Ind. Electron.*, 2013, **60**, (1), pp. 339–349

[27] Ayachit, A., Corti, F., Reatti, A., *et al.*: 'Zero-voltage switching operation of transformer class-E inverter at any coupling coefficient', *IEEE Trans. Ind. Electron.*, 2018. Early access: doi: 10.1109/TIE.2018.2838059

[28] Wireless Power Consortium, June 2013. Available at http://www.wirelesspowerconsortium.com, accessed July 2014

[29] WE-WPCC Wireless Power Charging Coil 760308110.Datasheet, Wurth Elektronik, Niedernhall, Germany, 2013

[30] https://www.mouser.co.uk/epcos/?gclid=EAIaIQobChMI-MCayOjY3gIV0OJ3Ch306A2aEAAYASAAEgLLNPD_BwE